Journal of Environmental Monitoring

Dynamic Article Links

Cite this: *J. Environ. Monit.*, 2012, **14**, 3174

www.rsc.org/jem

PAPER

Absorption Ångström exponents of aerosols and light absorbing carbon (LAC) obtained from *in situ* data in Covilhã, central Portugal

S. Mogo,*[abc] V. E. Cachorro,[a] A. de Frutos[a] and A. Rodrigues[b]

Received 2nd May 2012, Accepted 18th October 2012
DOI: 10.1039/c2em30345k

A field campaign was conducted from October 2009 to July 2010 at Covilhã, a small town located in the region of Beira Interior (Portugal) in the interior of the Iberian Peninsula. The ambient light-absorption coefficient, σ_a (522 nm), obtained from a Particle Soot Absorption Photometer (PSAP), presented a daily mean value of 12.1 Mm^{-1} (StD = 7.3 Mm^{-1}). The wavelength dependence of aerosol light absorption is investigated through the Ångström parameter, α_a. The α_a values for the pair of wavelengths 470–660 nm ranged from 0.86 to 1.47 during the period of measurements. The PSAP data were used to infer the mass of light absorbing carbon (LAC) and the daily mean varied from 0.1 to 6.8 μg m^{-3}. A detailed study of special events with different aerosol characteristics is carried out and, to support data interpretation, air masses trajectory analysis is performed.

1 Introduction

The climatic effect of aerosols depends strongly on their optical properties. In fact, recent research shows that the understanding of aerosol effects on climate requires information not only on the aerosol amount, but also on aerosol characteristics such as size, composition and optical properties, especially including absorption, which is the least known. Further, knowledge of the connection between the chemical composition and the measured optical properties of the aerosols is largely absent.

Reduction in the intensity of a direct solar beam during its propagation through the atmosphere is determined by absorption and scattering processes. These two different mechanisms contribute to extinction of light, a term that means the loss of light in the atmosphere from a directly transmitted beam. The absorption, measured by the light absorption coefficient, σ_a, is primarily attributed to sub-micron carbon particles at solar radiation wavelengths. Light absorbing carbon (LAC) is an anthropogenic component of atmospheric aerosols produced by incomplete combustion of fossil fuel and biomass burning. On the other hand, scattering mainly arises from sulfate and nitrate aerosols from anthropogenic sources and is measured by the scattering coefficient, σ_s. It has also been suggested that the organic species, biogenic scattering aerosols and several other particles play important roles in aerosol light scattering.[1] The extinction coefficient, σ_e, is obtained from $\sigma_e = \sigma_s + \sigma_a$.

The wavelength dependence of the aerosol extinction coefficients is traditionally studied using a parameter named Ångström exponent, α. This parameter was introduced by Ångström[2] and subsequently used to represent the turbidity of the atmosphere and to model the effect of aerosols on solar radiation.[3] It is defined as the negative slope of the logarithm of extinction coefficient as a function of wavelength and is given by:

$$\sigma_e = K\lambda^{-\alpha_e}. \quad (1)$$

[a]*Grupo de Óptica Atmosférica, Univ. Valladolid, Valladolid, Spain. E-mail: sipmogo@gmail.com*
[b]*Universidade da Beira Interior, Covilhã, Portugal*
[c]*Instituto Dom Luis, Portugal*

Environmental impact

Automated instruments such as particle soot absorption photometers (PSAPs), aethalometers and nephelometers have become usual in practice, allowing for the continuous obtainment of spectrally resolved optical properties of aerosols. The spectral variation of these properties is a valuable tool to infer the particles chemical composition and size. We present a methodology to study the spectral dependence of the absorption data that can be used to infer the composition of the particles when no chemical data are available. However, the data obtained from a PSAP need to be corrected with data obtained from a nephelometer and not always an absorption and a scattering instrument are simultaneously available. In this work we also present a method for obtaining scattering corrected absorption coefficients of aerosols.

The same concept has also been applied to the scattering and the absorption of light:

$$\sigma_s = K'\lambda^{-\alpha_s}, \quad (2)$$

$$\sigma_a = K''\lambda^{-\alpha_a}. \quad (3)$$

The wavelength dependence of the aerosol scattering coefficients (scattering Ångström exponent, α_s) has proved useful in deriving aerosol size information.[4,5] Also, the wavelength dependence of the aerosol absorption coefficients (absorption Ångström exponent, α_a) appears to be related to the aerosol composition, and thus to the sources of aerosols.[6–10] α_a values near 1 have been found in urban-industrial aerosols (dominated by black carbon), larger α_a values in biomass burning aerosols and the largest α_a values in desert dust aerosols.[11,12] Other studies show that the α_a for organic species (sometimes called brown carbon) is larger than that for black carbon[13] and can depend on the wavelength (increasing for decreasing wavelength), whereas it is independent of wavelength for black carbon.

The use of the Ångström exponents $\alpha_{s,a}$ has significantly increased in the last few years, because this parameter is easily estimated using automated *in situ* instrumentation and automated surface sun photometry.

In this work, we present data obtained at Covilhã, a small town located in the region of Beira Interior (Portugal) in the interior of the Iberian Peninsula. The campaign was conducted from October 2009 to July 2010 and was designed to obtain experimental data for local aerosols, their absorbent characteristics and their effects on radiative forcing. For this purpose different instruments were simultaneously installed in the University of Beira Interior facilities. In this work we will focus mainly on the absorption Ångström exponents of aerosols. The light absorption coefficient of the aerosols, σ_a, was measured continuously using a three-wavelength Particle Soot Absorption Photometer (PSAP), in near real time. The mass of light absorbing carbon was obtained as a relevant information for air quality management.

2 Methods

2.1 Site description

The particles analyzed in this study were collected within the urban environment of Covilhã, a town in central Portugal. The town proper has ~36 700 inhabitants, and the municipality has an area of 555.6 km^2 with a total population of ~53 500. Located in the proximity of the mountains (Serra da Estrela, 2000 m a.s.l.), Covilhã towers between 450 and 800 m a.s.l., and is one of the main urban centers of the Beira Interior region. In the immediate vicinity of the town, the mountains are enveloped by forested areas dominated by varieties of pine and chestnut trees, and the valley is dominated by agriculture in small farms.

The sampling site is located on the terrace of a six-storey building in the University of Beira Interior facilities, 150 m from the city center. This site (40°16′39.63″N, −7°30′32.48″W, 625 m a.s.l.) is at an altitude of about 18 m above the street level, unobstructed for all wind directions and with no nearby sources at the roof level. The closest street with significant road traffic passes immediately in front of the building. The urban aerosol is typical of a lightly industrialized town whose contamination mostly stems from road traffic and domestic heating; however, as yet no emission source inventory has been developed for this town.

The climate in Covilhã is temperate, moderately cold in the winter and relatively warm in the summer. The monthly variations of surface meteorological parameters like temperature, relative humidity, wind speed along with total rainfall over the study period are shown in Fig. 1. The data were obtained from an unofficial meteorological[14] station located ~200 m from our terrace. Unfortunately no other meteorological data are available closer to our laboratory.

The average temperature was found to be 12.0 °C with a minimum of 5.5 °C during January and a maximum of 25.8 °C during July. In general, the relative humidity was high across the study period with an average of 64%. The warmer seasons remained moderately dry with an average relative humidity of 49% compared to the cold seasons with an average relative humidity of 72%. The total rainfall during the entire study period

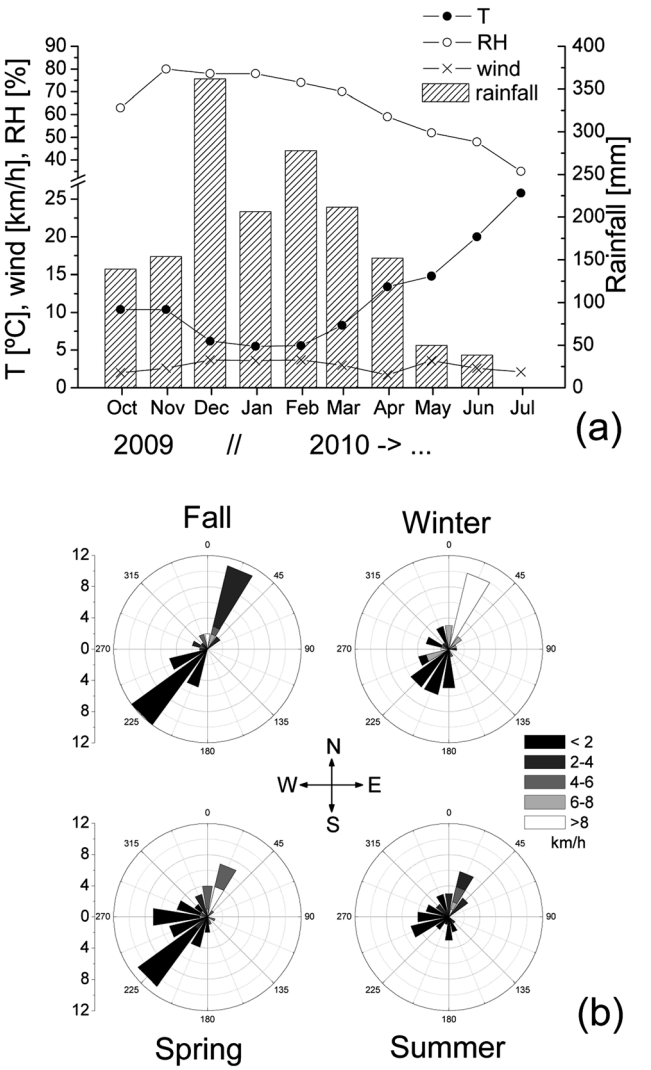

Fig. 1 (a) Seasonal variations of temperature, wind speed, relative humidity and rainfall over the station. (b) Rose diagrams of surface wind speed and direction over the entire study period in Covilhã.

was found to be 637 mm, 53.2% of which was during winter (846.1 mm) with scanty or no rainfall during summer (38.3 mm). The surface wind pattern was mainly north northeasterly with an average speed of 3 km h^{-1} but in fall and spring a southwest component was also registered.

2.2 Instrumentation

For transferring aerosols from the outside of the laboratory building to the inside, an inlet protected with a rain cap was used. The system limits the size of the collected particles, selecting only the fine fraction and excluding the coarse. The cut-off diameter of the inlet nozzle and sample transport line was approximately 2.5 μm and the airflow through the sampling line was divided into two separate flows and directed toward individual instruments. After collection, two methods were used for determination of the absorption coefficients: an automated method, the PSAP, and a manual system named IS3 (Integrating Sphere Spectral System).

For the automated method, the light absorption coefficients were measured at three wavelengths (470, 522 and 660 nm) with a commercial PSAP working with the air flow set to 1.5 l min^{-1}. The instrument uses a filter-based technique in which aerosols are continuously deposited onto a glass fiber filter at a known flow rate. The change in the transmitted light is related to the optical absorption coefficient using Beer's law. The instrument is an improved version of the integrating plate method[15] and is described in detail by Bond *et al.*[16] and Virkkula *et al.*[17] The resolution precision of the PSAP instrument is limited to ± 0.05 Mm^{-1}.[18,19]

For the manual system, the IS3,[8] the particles are collected over polycarbonate membrane filters using an in-line filter holder. Subsequently, the filters with their aerosol loads are dissolved in chloroform to produce a liquid suspension of the deposited particles. This suspension is placed in the center of an integrating sphere into a quartz cell, where it is irradiated with both direct light from the source and uniformly distributed light within the sphere. If an absorbing substance is present in the sample, the signal decreases. As the real part of the refractive index of chloroform is nearly the same as that of suspended particles, the light scattering is highly reduced. Thus, decreases in the light signal can be attributed only to absorption. Using the measurement of the light transmitted intensity, the absorption coefficients are then determined assuming that the attenuation of the beam follows the Beer–Lambert law. Besides the advantage of the refractive index, the chloroform was selected because it does not react with most aerosol components but instead it will dissolve completely the polycarbonate filter. The relative accuracy of the absorption coefficient measured by the IS3 instrument is estimated to be around 3%.[8] The system is fully described by Montilla *et al.*[8]

2.3 Data processing

The averaging time of the PSAP was 60 s and the filter was replaced whenever the amount of transmitted light achieved 70% of the initial intensity. Hourly averages are accepted if the variation is less than 50% and daily averages are accepted if more than 18 hourly averages are available. The response of the PSAP

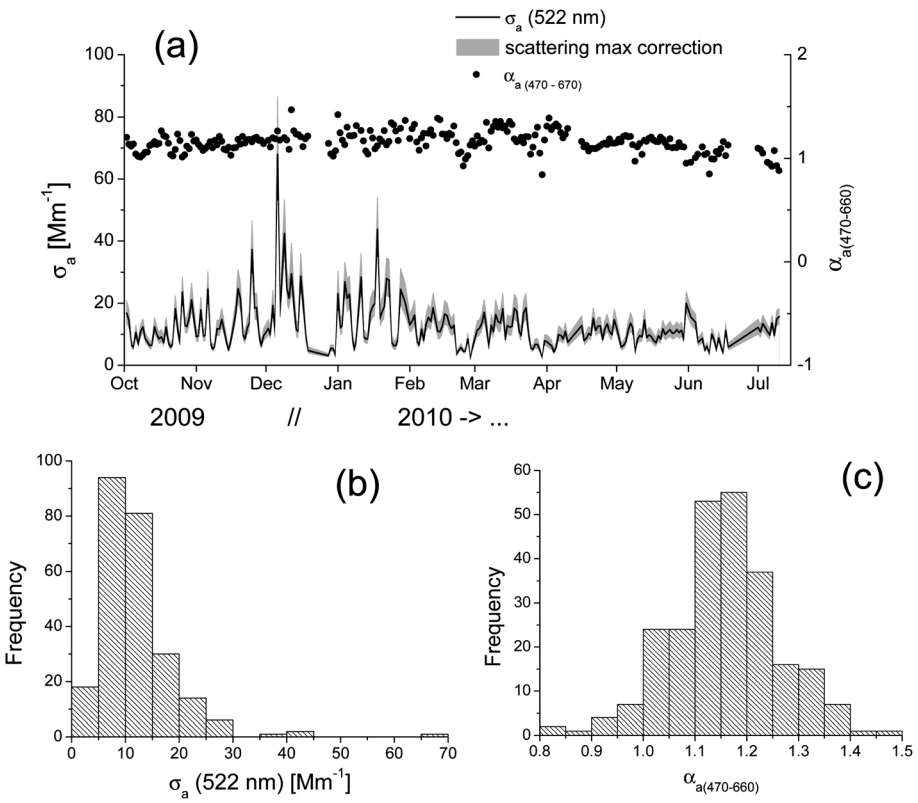

Fig. 2 (a) Time series of the σ_a (522 nm) and the $\alpha_{a(470–660)}$ for all dataset (24 h averages). Frequency histogram for the (b) absorption coefficient and (c) absorption Ångström exponent.

depends on the loading of particles on the filter, on the amount of light scattered by the particles, on the flow rate and on the spot size.[16,17] The data were corrected for these dependencies by using the data provided by the IS3.

The samples for analysis using the IS3 were collected on 47 mm Millipore polycarbonate membrane filters with homogeneous size distribution pores of 0.2 μm. The filters were collected for 24 h periods with a constant flow rate of 15 l min^{-1}. The IS3 is capable of covering the spectral wavelength range of 320–800 nm with a variable spectral resolution but only limited temporal resolution. The time-resolution is dependent on the filter-sampling time. The main inconvenience of the IS3 system is its labor-intensity and the low achievable temporal resolution.

The PSAP data are nearly continuous but not scattering corrected while the IS3 data are only 24 h resolved but are scattering corrected. Both together allow for a nearly continuous data series with a good estimation of the influence of scattering. As simultaneous measurements from both instruments were available we were able to determine the maximum and minimum influence of scattering in the PSAP results. This range of values, observed during the whole period of measurement, is shown in Fig. 2(a) as a shaded area and the average difference obtained was used to correct the PSAP data.

For investigating the wavelength dependence of σ_a, we calculated $\alpha_{a(\lambda_1,\lambda_2)}$ for a pair of wavelengths, λ_1, λ_2, according to the following formula:

$$\alpha_a = -\frac{\log\left(\sigma_{a(\lambda_2)}/\sigma_{a(\lambda_1)}\right)}{\log(\lambda_2/\lambda_1)}, \quad (4)$$

and we calculated $\alpha_{a(\lambda_1,\lambda_2,\ldots,\lambda_n)}$ for more than two wavelengths through the logarithmic fit of eqn (3).

To convert the aerosols light absorption coefficients into the mass of LAC we assumed that all light absorption was due to LAC and all LAC had the same mass absorption specific coefficient, $B_a = \sigma_a M_{LAC}^{-1}$. The *in situ* LAC absorption specific coefficient was obtained from the IS3 after calibration with an industrially produced pigment (nigrosin, Sigma-Aldrich). For 24 h samples, the detection limit of the IS3 in terms of aerosol mass concentrations was established to be 4% and the measurement uncertainty is about 10% maximum.[8] As the absorption specific coefficient obtained from the IS3 remained within this 10% uncertainty around the commonly accepted value of 10 m^2 g^{-1},[20,21] we decided to use this value in our LAC estimations.

Absorption coefficients, absorption Ångström exponents and LAC data are available from 9th October 2009 to 31st July 2010 and the statistical data are calculated based on the daily averages.

3 Results and discussion

3.1 Temporal variations in aerosol absorption properties and LAC

During our observations, the daily mean value of σ_a at 470 nm, 522 nm and 660 nm ranged from 1.6 to 81.4 Mm^{-1}, 1.3 to 67.9 Mm^{-1} and 1.1 to 53.0 Mm^{-1} (average 14.2, 12.1 and 9.6 and standard deviation 8.6, 7.3 and 5.7 Mm^{-1}), respectively. The daily mean values of $\alpha_{a(470–660)}$ ranged from 0.84 to 1.47 (average 1.16 and standard deviation 0.10). For σ_a the median value is lower than the mean while for $\alpha_{a(470–660)}$ the median equals the

Table 1 Evaluation of the overall ranges and median values of the absorption coefficients, the Ångström exponents and LAC obtained from the dataset measured at Covilhã

		Min.	Max.	Mean	Median	StD	P25	P75
σ_a [Mm^{-1}]	470 nm	1.6	81.4	14.2	12.5	8.6	9.3	16.9
	522 nm	1.3	67.9	12.1	10.8	7.3	7.9	14.2
	660 nm	1.1	53.0	9.6	8.5	5.7	6.2	11.3
α_a(470–522)		1.06	2.05	1.53	1.53	0.16	1.43	1.62
α_a(522–660)		0.70	1.21	0.99	1.00	0.08	0.95	1.04
α_a(470–660)		0.84	1.47	1.16	1.16	0.10	1.10	1.21
α_a(470–522–660)		0.82	1.43	1.13	1.13	0.10	1.08	1.19
LAC [μg m^{-3}]		0.1	6.8	1.2	1.1	0.7	0.8	1.4

Table 2 Seasonal variations in monthly averaged aerosol absorption coefficients at 522 nm and absorption Ångström exponents for the wavelengths pair 470 nm/670 nm

σ_a 522 nm					α_a 470–660			
Month	Min.	Max.	Mean	StD	Min.	Max.	Mean	StD
Oct	5.8	23.6	11.0	4.6	1.01	1.27	1.12	0.07
Nov	4.8	37.3	12.9	7.1	1.03	1.21	1.14	0.05
Dec	**2.4**	**67.9**	**17.9**	**15.3**	**1.02**	**1.47**	**1.18**	**0.10**
Jan	**4.8**	**43.8**	**17.0**	**9.1**	**1.04**	**1.42**	**1.22**	**0.09**
Feb	**1.3**	**18.5**	**10.4**	**4.7**	**0.93**	**1.39**	**1.19**	**0.11**
Mar	1.9	18.5	11.4	4.5	0.84	1.36	1.21	0.11
Apr	4.3	15.1	9.9	2.8	1.07	1.39	1.19	0.09
May	3.5	20.0	10.0	2.9	0.95	1.22	1.14	0.06
Jun	**3.3**	**15.6**	**7.9**	**3.6**	**0.85**	**1.16**	**1.04**	**0.08**
Jul	**9.7**	**15.7**	**12.3**	**2.2**	**0.88**	**1.10**	**0.99**	**0.08**

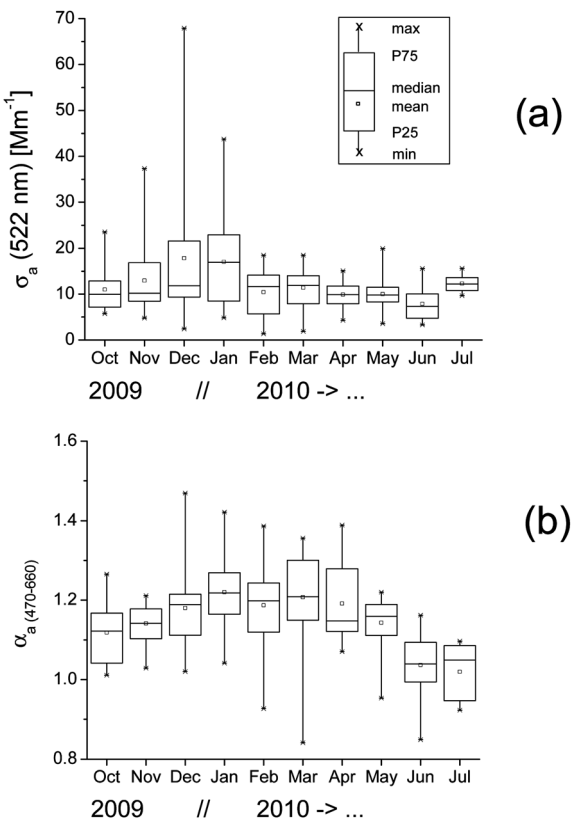

Fig. 3 Seasonal variations of (a) σ_a (522 nm) and (b) $\alpha_{a(470–660)}$ over Covilhã.

Table 3 Seasonal variations in monthly averaged LAC

LAC [μg m^{-3}]				
Month	Min.	Max.	Mean	StD
Oct	0.6	2.3	1.1	0.5
Nov	0.5	3.7	1.3	0.7
Dec	**0.2**	**6.8**	**1.8**	**1.5**
Jan	**0.5**	**4.4**	**1.7**	**0.9**
Feb	**0.1**	**1.8**	**1.0**	**0.5**
Mar	0.2	1.8	1.1	0.5
Apr	0.4	1.5	1.0	0.3
May	0.4	2.0	1.0	0.3
Jun	**0.3**	**1.6**	**0.8**	**0.4**
Jul	**1.0**	**1.6**	**1.2**	**0.2**

mean. The $\alpha_{a(470–522)}$ is higher than $\alpha_{a(522–660)}$ and for the three wavelengths, 470 nm/522 nm/660 nm, $\alpha_{a(470–522–660)}$ is smaller than that for the pair of wavelengths 470 nm/660 nm, $\alpha_{a(470–660)}$. The statistics on σ_a and α_a values is presented in Table 1 and a time series representing over 274 days of measurement is shown in Fig. 2(a). The frequency histogram of σ_a and α_a, shown in Fig. 2b and c, presents only one frequency mode, centered at 7.5 Mm^{-1} and 1.18 Mm^{-1}, respectively, for each parameter.

The σ_a and α_a values observed in our study are comparable to those in other urban not heavily populated regions, such as those presented by Heintzenberg and Bussemer[22] at Melpitz ($\sigma_a(550) =$ ~8 to 65 Mm^{-1}) and Mogo *et al.*[23] at Valladolid ($\sigma_a(550) = 7.3$–101.4 Mm^{-1}, $\alpha_{a(400–650)} = 0.1$–1.3).

Even though a complete annual dataset is not available, we consider it still possible to analyze the seasonal cycle through the monthly means, as data are available for all seasons: spring (complete, Mar, Apr, May), summer (only 2 months, Jun, Jul), fall (only 2 months, Oct, Nov) and winter (complete, Dec, Jan, Feb).

The seasonal and monthly mean values of σ_a and α_a are delineated in Table 2. Fig. 3 shows a marked seasonal cycle in the monthly averaged values of both parameters, with higher values registered during the cold seasons and smaller values registered during the warm seasons. This fact is probably related to the domestic heating. Statistical data regarding LAC values are presented in Table 3, showing also this seasonal cycle. Although no emission source inventory has been developed for this city, we suggest domestic heating as a possible reason for seasonal averages, based on our knowledge of local habits. Home heating systems include wood-burning fireplaces, electric baseboard heaters and oil/natural gas furnaces.

3.2 Relationships between aerosol parameters

In Fig. 4(a) we present the correlation between the absorption in the different channels. The relation between channels describes the proportion of the measurements for different wavelengths and each pair of measurements should obey eqn (3). In this way, the slope of the linear fit for each correlation is $(\lambda_1/\lambda_2)^{-\alpha_a}$ and, for each pair of wavelengths, the respective Ångström exponent can be calculated. From the figure it is clear that for absorption coefficients one line is enough to correlate the different channels, indicating the presence of only one main absorber. This main absorber presents an absorption Ångström exponent near 1.18 as observed in the frequency histogram of the α_a parameter

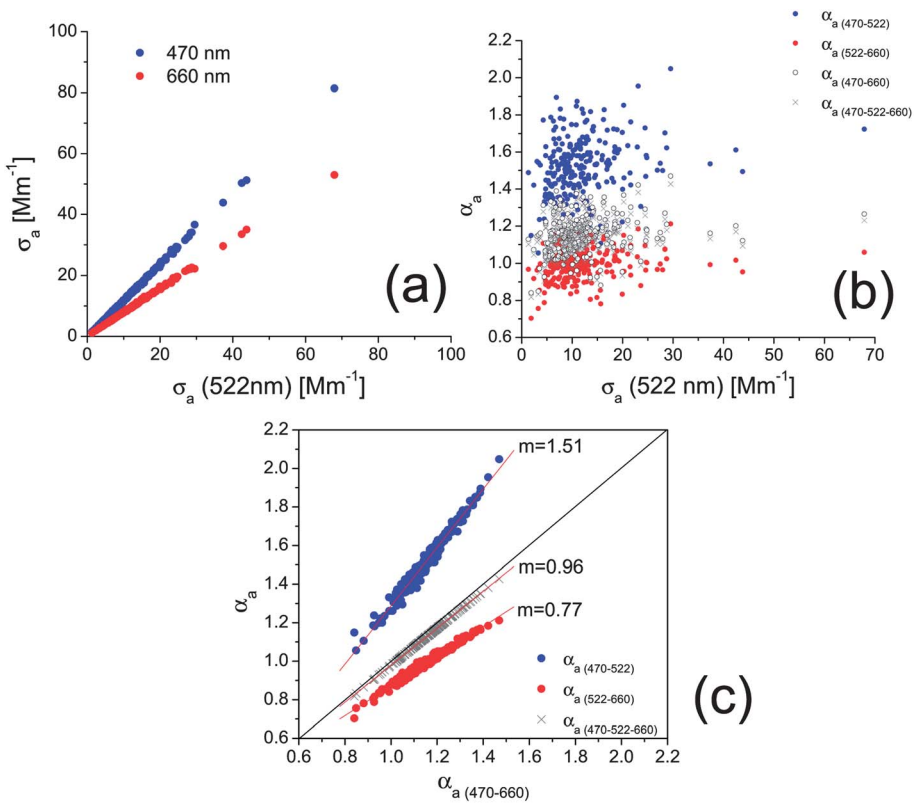

Fig. 4 Relationships between aerosol parameters.

(Fig. 2(c)). This behavior is not usual for the scattering or the extinction Ångström exponents, where two lines with two different slopes are commonly observed. Since the slopes of the lines depend on the particle size, these two lines represent the presence of two different particle sizes and the frequency histograms present two modes (usually, fine and coarse modes). See for example Mogo *et al.*[24]

Also in Fig. 4(b), we present the relation between the absorption coefficients and the respective Ångström exponents, showing the dispersion of the values. The Ångström exponents were calculated for the pairs of wavelengths 470 nm/522 nm, $\alpha_{a(470–522)}$, 522 nm/660 nm, $\alpha_{a(522–660)}$, 470 nm/660 nm, $\alpha_{a(470–660)}$ and also for the set 470 nm/522 nm/660 nm, $\alpha_{a(470–522–660)}$. There is a lack of universality in the literature as no reference wavelengths exist and different authors present the Ångström exponent data for different pairs or sets of wavelengths (mainly depending on the instruments used). We decided to present all the possibilities, not only to study the behavior of the absorption coefficient across the spectrum, but also to compare the α_a values with each other. The Ångström exponents are higher for the pair of wavelengths 470 nm/522 nm and smaller for the pair 522 nm/660 nm, defining in this way the shape of the absorption spectra: decreases quickly on the 470 nm/522 nm range and decreases less abruptly on the 522 nm/660 nm range. As a consequence, the absorption coefficient becomes more sensitive to spectral variations at low wavelengths than at high wavelengths of the spectrum. Taking the extreme wavelengths of our spectral range, the Ångström exponents obtained, $\alpha_{a(470–660)}$, are similar to those obtained by adjusting with three wavelengths, $\alpha_{a(470–522–660)}$.

The dependence of σ_a on wavelength is further examined in Fig. 4(c) by analyzing the relation between the Ångström exponents for different pairs of wavelengths. In Fig. 4(c), the Ångström exponents for the pair of wavelengths 470 nm/660 nm, $\alpha_{a(470–660)}$, are related to the Ångström exponents for all the other pairs, $\alpha_{a(470–522)}$, $\alpha_{a(522–660)}$ and $\alpha_{a(470–522–660)}$. The pair 470 nm/660 nm is emphasized because these are our extreme wavelengths. The slope of the linear fit for each correlation is presented, showing values above one for the $\alpha_{a(470–522)}$, 1.51, and below one for the $\alpha_{a(522–660)}$, 0.77, as expected from the analysis

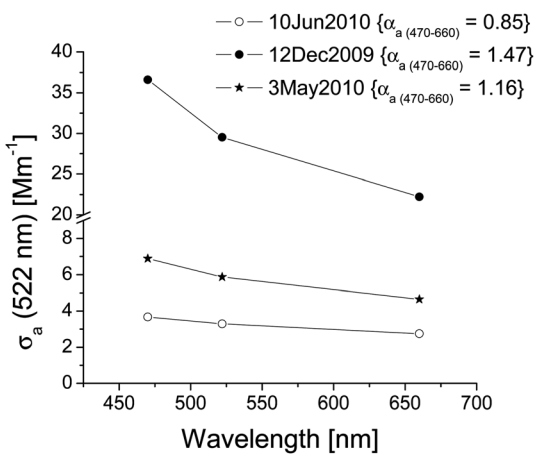

Fig. 5 Aerosol σ_a variation along the visible spectrum. The different lines belong to three example days: one particularly high, 12 December (●); one particularly low, 10 June (○); and one normal day, 3 May (★).

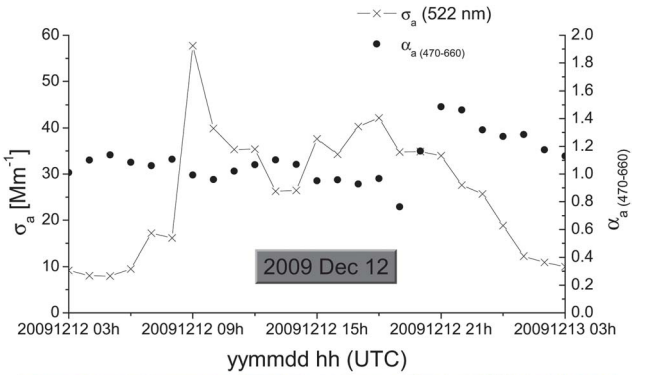

Fig. 6 Possible long range transport of dust aerosol.

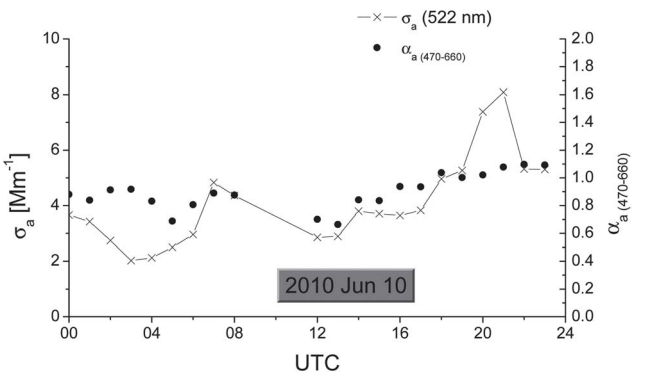

Fig. 7 Air mass transported from the Arctic.

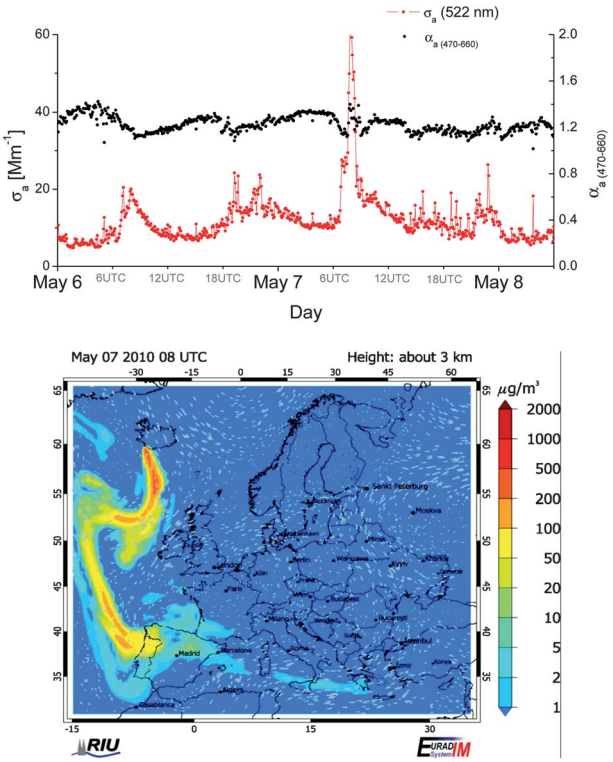

Fig. 8 Arrival of aerosol to the observational site from the eruption of the Icelandic volcano Eyjafjallajökull.

of the previous figures. Using three wavelengths for the determination of $\alpha_{a(470–522–660)}$ decreases slightly the values obtained with respect to $\alpha_{a(470–660)}$ (slope of the linear fit 0.96).

3.3 Special events

In the analysis presented here, we focus on the data from days with specific aerosol characteristics. And for each case study we report the absorption coefficients of the aerosol and its absorption Ångström exponent.

In Fig. 5 we present the spectral shape variation of absorption coefficients throughout the spectrum. The three curves presented belong to three example days: one exceptionally high (Dec 12), one particularly low (Jun 10) and the last with the normal atmospheric condition of the area (May 3). As shown in Fig. 5 the absorption coefficient decreases with wavelength, the smaller the wavelength the higher the absorption coefficient. This decrease, however, is not very pronounced, as a result also of Fig. 4.

On 2009 December 12, a significantly higher value of σ_a compared to that measured on the previous days was obtained. The meteorological conditions were stable, with average temperature 9.2 °C (minimum 4.7 °C at 22 : 06, maximum 15.6 °C at 12 : 09). The wind speed was very low during the event (around 1.9 km h^{-1}, from SW) and the relative humidity ranged from 41% at 12 : 13 to 97% at 23 : 57. On the basis of back trajectories, the HYSPLIT transport model[25,26] indicates that the air sampled in Covilhã throughout this period was transported from the south, with dust arriving from north Africa. Fig. 6 shows the hourly averaged absorption coefficients registered during the event. The maximum value ($\sigma_a = 57.7$ Mm^{-1}, 522 nm) occurred at noon but values remained high the rest of the day. The daily absorption Ångström exponent for the pair of wavelengths 470 nm/660 nm was 1.21, maximum 1.50 and minimum 0.76. On the basis of the data registered, the event may have been related to the long range transport of dust and probably combined with local sources. Unfortunately the presence of clouds prevented the use of the AERONET network of CIMEL photometers to confirm this event. Also MODIS data are difficult to interpret due to the same reason, however, these data likewise support the possibility of a dust event.

On 2010 June 10, the lower value of σ_a compared to that measured on the previous days was attributed to the arrival of a clean air mass. The average temperature was 12.9 °C (minimum 9.9 °C at 23 : 46, maximum 19.1 °C at 17 : 20). The wind was from NW with average speed 2.8 km h^{-1} and the relative humidity ranged from 37% at 16 : 41 to 97% at 09 : 41. Back-trajectory modeling revealed that the air mass was transported from the Arctic under the unique influence of the high latitudes of the North Atlantic Ocean. Fig. 7 shows the hourly averaged absorption coefficients registered during that day. The σ_a remained low during all day, average 4.1 Mm^{-1} at 522 nm, and only a small peak at night, reaching a maximum value of 8.1 Mm^{-1}. The daily absorption Ångström exponent for the pair of wavelengths 450 nm/652 nm was 0.90, maximum 1.11 and minimum 0.67.

Other interesting event occurred in May. Beginning on 14th April 2010, the eruption of the volcano Eyjafjallajökull, Iceland, caused enormous disruption to air travel across western and northern Europe. The data discussed here concern the period between 6 and 8 May 2010, when the ash plume reached the Iberian Peninsula. The HYSPLIT transport model indicates that the air sampled in Covilhã throughout this period was transported from the north, with ash arriving from Iceland. Also the vertical profile and the mixed layer depth were obtained from the model. Fig. 8 shows time series of the PSAP corrected data at Covilhã together with the size resolved concentration of particles obtained from the EURopean Air Pollution Dispersion (EURAD) model from the Rhenish Institute for Environmental Research at the University of Cologne. The arrival time of the air mass occurred during the peak of the morning rush hour, which prevented us from knowing the exact impact of the volcanic ash on the measurements. However, comparison of the σ_a 5-minute averages obtained during the morning rush hour for all the measurements period and for 7th May showed that the absorption coefficient doubles its value. 30.1 Mm^{-1} for May 7 and 15.2 Mm^{-1} for all other days. On 7th May the σ_a 5-minute averages reached a maximum value of 66.0 Mm^{-1} at 522 nm around 8 UTC and the Ångström exponent for the pair of wavelengths 470 nm/660 nm was 1.35.

Comparing the Ångström exponents for the three events shows that the highest values were registered for the dust event and the lowest values were registered for the air mass transported from the Arctic. The shape of the spectral absorption coefficients is also different, with a stronger dependence on the wavelength for the day of the dust event.

4 Concluding remarks

We have initiated a database of aerosol properties for Covilhã, where no previous studies had been performed. The PSAP and

the IS3 were used together, allowing an automated measurement of the absorption coefficients corrected from scattering. The daily mean values of σ_a registered at 522 nm ranged from 1.3 Mm^{-1} to 67.9 Mm^{-1} during the cold months and from 1.9 Mm^{-1} to 20.0 Mm^{-1} during the warmer months. The α_a values for the pair of wavelengths 470–660 nm ranged from 0.93 to 1.47 during the cold months and from 0.86 to 1.39 during the warmer months. The LAC values ranged from 1.0 μg m^{-3} to 1.8 μg m^{-3} during the cold station and ranged from 0.8 μg m^{-3} to 1.2 μg m^{-3} during the warmer station.

The concept of wavelength-dependent absorption Ångström exponents has been fully exploited. The alpha parameter was studied in all the possible pairs of wavelengths and the parameter was used to provide insight into the differentiation of aerosols. Although the α_a is a useful tool for helping to distinguish aerosol types, comparisons with the literature are quite difficult as this kind of data is scarce and different authors present data for different pairs of wavelengths.

Portions of the dataset containing aerosol characteristics from identifiable sources were selected for further analysis. The highest absorption coefficients were observed during 2009 December 12, with the σ_a levels 2.5× higher than their average. Back-trajectory modeling revealed that this air mass was transported from the south with dust arriving from north Africa and probably combined with local sources. The smaller absorption coefficients were registered during 2010 June 10, with air masses quickly arriving from the north Atlantic. May 6 to 7, 2010 were also selected for analysis as on this day the strongest arrival of particles from the eruption of the Icelandic volcano Eyjafjallajokull on April 14 was recorded.

Acknowledgements

This work was supported by the Integrated Action Portugal – Spain E-99/09 2009–2010. Financial support from the Spanish MICINN (projects of ref. CGL2008-05939-CO3-01/CLI and CGL2009-09740 and "Acción Complementaria" CGL2011-13085-E) is gratefully acknowledged.

References

1 P. Quinn, T. Miller, T. Bates, J. Ogren, E. Andrews and G. Shaw, *J. Geophys. Res.*, 2002, **107**, 4130.
2 A. Ångström, *Geogr. Ann.*, 1929, **11**, 156–166.
3 V. Cachorro, A. de Frutos and J. Casanova, *Appl. Opt.*, 1987, **26**, 3069–3076.
4 P. Russell, R. Bergstrom, Y. Shinozuka, A. Clarke, P. DeCarlo, J. Jimenez, J. Livingston, J. Redemann, O. Dubovik and A. Strawa, *Atmos. Chem. Phys.*, 2010, **10**, 1155–1169.
5 S. Pereira, F. Wagner and A. Silva, *Atmos. Chem. Phys.*, 2011, **11**, 17–29.
6 S. Mogo, V. Cachorro, M. Sorribas, A. de Frutos and R. Fernández, *Geophys. Res. Lett.*, 2005, **32**, L13811.
7 H. Moosmüller, R. Chakrabarty, K. Ehlers and W. P. Arnott, *Atmos. Chem. Phys.*, 2011, **11**, 1217–1225.
8 E. Montilla, S. Mogo, V. Cachorro and A. de Frutos, *J. Aerosol Sci.*, 2011, **42**, 204–212.
9 J. Sandradewi, A. Prévôt, M. Alfarra, S. Szidat, M. Wehrli, M. Ruff, S. Weimer, V. Lanz, E. Weingartner, N. Perron, A. Caseiro, K. Giebl, H. Puxbaum, L. Wacker and U. Baltensperger, *Atmos. Chem. Phys. Discuss.*, 2008, **8**, 8091–8118.
10 H. Gadhavi and A. Jayaraman, *Ann. Geophys.*, 2010, **28**, 103–111.
11 R. Bergstrom, P. Russell and P. Hignet, *J. Atmos. Sci.*, 2002, **59**, 567–577.
12 T. Bond and R. Bergstrom, *Aerosol Sci. Technol.*, 2006, **40**, 27–67.
13 M. Andreae and A. Gelencsér, *Atmos. Chem. Phys.*, 2006, **6**, 3131–3148.
14 MeteoCovilhã, MeteoCovilhã, http://www.meteocovilha.com, 2011.
15 C. Lin, M. Baker and R. Charlson, *Appl. Opt.*, 1973, **12**, 1356–1363.
16 T. Bond, T. Anderson and D. Campbell, *Aerosol Sci. Technol.*, 1999, **30**, 582–600.
17 A. Virkkula, N. Ahlquist, D. Covert, W. Arnott, P. Sheridan, P. Quinn and D. Coffman, *Aerosol Sci. Technol.*, 2005, **39**, 68–83.
18 S. Springston and A. Sedlacek III, *Aerosol Sci. Technol.*, 2007, **41**, 1110–1116.
19 T. Müller, J. Henzing, G. de Leeuw, A. Wiedensohler, A. Alastuey, H. Angelov, M. Bizjak, M. Collaud Coen, J. Engström, C. Gruening, R. Hillamo, A. Hoffer, K. Imre, P. Ivanow, G. Jennings, J. Sun, N. Kalivitis, H. Karlsson, M. Komppula, P. Laj, S.-M. Li, C. Lunder, A. Marinoni, S. Martins dos Santos, M. Moerman, A. Nowak, J. Ogren, A. Petzold, J. Pichon, S. Rodriquez, S. Sharma, P. Sheridan, K. Teinilä, T. Tuch, M. Viana, A. Virkkula, E. Weingartner, R. Wilhelm and Y. Wang, *Atmos. Meas. Tech.*, 2011, **4**, 245–268.
20 C. Liousse, H. Cachier and S. Jennings, *Atmos. Environ., Part A*, 1993, **27**, 1203–1211.
21 J. Martins, P. Hobbs, R. Weiss and P. Artaxo, *J. Geophys. Res.*, 1998, **103**, 32051–32067.
22 J. Heintzenberg and M. Bussemer, *J. Aerosol Sci.*, 2000, **31**, 801–812.
23 S. Mogo, V. Cachorro, M. Sorribas and A. de Frutos, *Opt. Pura Apl.*, 2006, **39**, 331–340.
24 S. Mogo, V. Cachorro, J. Lopez, E. Montilla, B. Torres, E. R. gues, Y. Bennouna and A. de Frutos, *Atmos. Chem. Phys.*, 2012, **12**, 5841–5857.
25 R. Draxler and G. Rolph, *Hybrid Single-Particle Lagrangian Integrated Trajectory Model Access* via *NOAA ARL Ready*, http://www.arl.noaa.gov/ready/hysplit4.html, NOAA Air Resources Laboratory, Silver Spring, MD, 2003.
26 G. Rolph, *Real-time Environmental Applications and Display System Ready*, http://www.arl.noaa.gov/ready/hysplit4.html, NOAA Air Resources Laboratory, Silver Spring, MD, 2003.